Quartz Crystal Microbalance Studies of Al_2O_3 Atomic Layer Deposition Using Trimethylaluminum and Water at 125 °C†

R. A. Wind[⊥,‡] **and S. M. George***[,‡,§]

Department of Chemistry and Biochemistry, Department of Chemical and Biological Engineering, University of Colorado, Boulder, Colorado 80309-0215

Received: May 27, 2009; Revised Manuscript Received: August 19, 2009

Al_2O_3 atomic layer deposition (ALD) growth with $Al(CH_3)_3$ (trimethylaluminum (TMA)) and H_2O as the reactants was examined at the relatively low temperature of 125 °C using quartz crystal microbalance (QCM) measurements. The total Al_2O_3 ALD mass gain per cycle (MGPC) and MGPCs during the individual TMA and H_2O reactions were measured versus TMA and H_2O exposures. The Al_2O_3 MGPC increased with increasing H_2O and TMA exposures at fixed TMA and H_2O exposures, respectively. However, the TMA and H_2O reactions were not completely self-limiting. The slower surface reaction kinetics at lower temperature may require very long exposures for the reactions to reach completion. The Al_2O_3 MGPCs increased quickly versus H_2O exposure and slowly reached limiting values that were only weakly dependent on the TMA doses. Small TMA exposures were also sufficient for the Al_2O_3 MGPCs to reach different limiting values for different H_2O doses. The TMA MGPCs increased for higher TMA exposures at all H_2O exposures. In contrast, the H_2O MGPCs decreased for higher TMA exposures at all H_2O exposures. This decrease may occur from more dehydroxylation at larger hydroxyl coverages after the H_2O exposures. The hydroxyl coverage after the H_2O exposure was dependent only on the H_2O exposure. The Al_2O_3 MGPC was also linearly dependent on the hydroxyl coverage after the H_2O dose. Both the observed hydroxyl coverage versus H_2O exposure and the Al_2O_3 ALD growth versus H_2O and TMA exposures were fit using modified Langmuir adsorption isotherm expressions where the pressures are replaced with exposures. These results should be useful for understanding low-temperature Al_2O_3 ALD, which is important for coating organic, polymeric, and biological substrates.

1. Introduction

Atomic layer deposition (ALD) is a thin film deposition technique that can fabricate ultrathin, continuous, and conformal films on very complex shapes. ALD is based on two sequential, self-limiting surface reactions.[1,2] Al_2O_3 ALD is one of the most widely investigated ALD systems.[3−12] Al_2O_3 ALD typically utilizes $Al(CH_3)_3$ (trimethylaluminum (TMA)) and H_2O as reactants.[13,14] The growth is nearly self-limiting for temperatures of 30−300 °C, no residual carbon is incorporated into the film, and the only reaction byproduct is CH_4. Al_2O_3 ALD displays almost all the requirements for ideal ALD.

The surface chemistry of the binary reaction sequence during Al_2O_3 ALD can be described as[12,15]

$$\text{(A)}\quad \mathrm{A1(OH)}_x^* + \mathrm{A1(CH_3)_3} \rightarrow \mathrm{A1O}_x\mathrm{A1(CH_3)}_{3-x}^* + x\mathrm{CH_4} \quad (1)$$

$$\text{(B1)}\quad \mathrm{A1O}_x\mathrm{A1(CH_3)}_{3-x}^* + (3-x)\mathrm{H_2O} \rightarrow \mathrm{A1O}_x\mathrm{A1(OH)}_{3-x} + (3-x)\mathrm{CH_4} \quad (2)$$

$$\text{(B2)}\quad (2x-3)\mathrm{A1OH}^* \leftrightarrow (x-1.5)\mathrm{A1OA1}^* + (x-1.5)\mathrm{H_2O} \quad (3)$$

where the asterisks indicate the surface species. These equations are written for one Al site for steady-state Al_2O_3 ALD growth. One Al atom is deposited during each reaction cycle.

The reaction of TMA with surface OH* (hydroxyl) species is given by reaction A in eq 1. x is the number of OH* species per Al site that react with each TMA molecule. The H_2O reaction occurs by direct replacement of CH_3^* (methyl) species with OH* species, as indicated by reaction B1 in eq 2. Stoichiometric Al_2O_3 is produced by only reactions A and B1 when $x = 1.5$. Reaction B2 in eq 3 is required to maintain stoichiometric Al_2O_3 if $x > 1.5$ or $x < 1.5$. When $x > 1.5$, AlOH* species undergo dehydroxylation to produce H_2O. When $x < 1.5$, H_2O dissociatively adsorbs on a dehydroxylated AlOAl* site to produce AlOH* species. Reaction B2 in eq 3 runs in reverse when $x < 1.5$.

Confirmation of these surface reactions is provided by Fourier transform infrared (FTIR) spectroscopy,[3−5] quartz crystal microbalance (QCM),[12,16] and quadrupole mass spectrometry (QMS)[8,12] studies. FTIR spectroscopy monitors the OH* and CH_3^* surface species and their interconversion during the TMA and H_2O reactions.[3−5] QCM measures the mass change during the TMA and H_2O reactions.[12,16] QMS observes the production of CH_4 as the primary gas phase reaction products.[8,12] The surface reactions have also been shown to be self-limiting.[3,9] Self-limiting growth allows ALD to produce conformal and atomically flat films on spatially complex substrates.[4,17,18] The

† Part of the "W. Carl Lineberger Festschrift".

* Corresponding author. E-mail: steven.george@colorado.edu.
‡ Department of Chemistry and Biochemistry.
§ Department of Chemical and Biological Engineering.
⊥ Current address: Synkera Technologies, Inc., 2021 Miller Dr., Longmont, CO 80501.

10.1021/jp9049268
Published on Web 09/16/2009

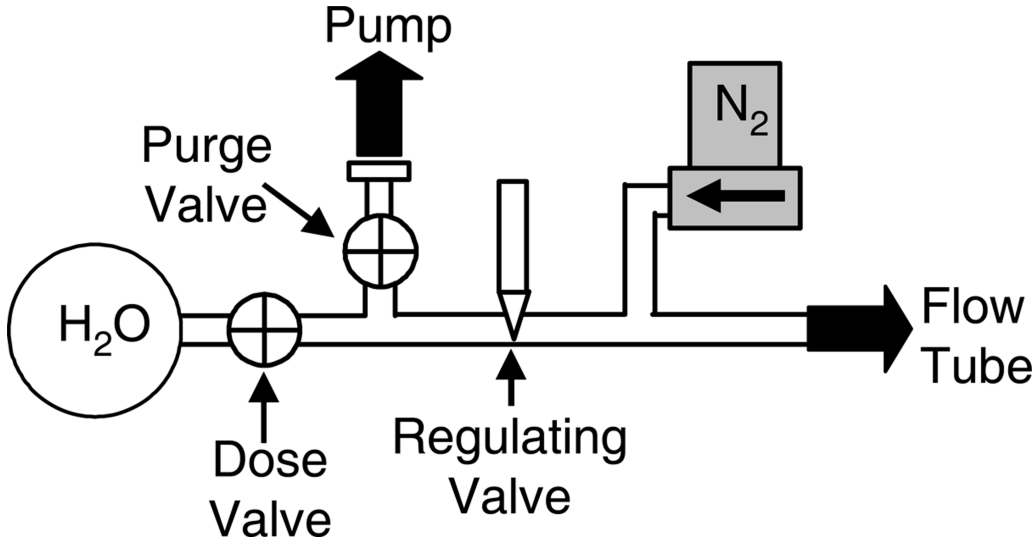

Figure 1. Diagram of the gas switching valves used for H_2O dosing.

Al_2O_3 ALD reaction is also able to initiate Al_2O_3 growth on a wide variety of surfaces, including oxides, nitrides, metals, semiconductors, and polymers.[4−6,19]

The thermochemistry of Al_2O_3 ALD is very favorable. The heat of reaction for $2Al(CH_3)_3 + 3H_2O \rightarrow Al_2O_3 + 6CH_4$ is −376 kcal.[20] This large exothermicity helps enable Al_2O_3 ALD at low temperatures. Al_2O_3 ALD is operative at temperatures as low as 33 °C.[7] Investigations have shown that Al_2O_3 ALD yields very well-defined films from 33 to 177 °C.[7] The low temperatures have allowed Al_2O_3 ALD to deposit on a range of thermally fragile substrates, such as organic, polymeric, and biological substrates.[7,19,21,22] These low-temperature Al_2O_3 ALD films are particularly useful for gas diffusion barriers on polymer substrates.[23−25]

Because of the importance of low-temperature Al_2O_3 ALD, this paper explores the dependence of Al_2O_3 ALD on H_2O and TMA exposures at 125 °C. These investigations are conducted using QCM studies. The total Al_2O_3 ALD mass gain per cycle (MGPC) is examined versus H_2O and TMA exposures. The separate MGPCs after the H_2O and TMA doses are also explored versus the H_2O and TMA exposures. The MGPCs provide information on the coverage of the OH* and CH_3^* surface species and the deposited Al coverage per cycle during Al_2O_3 ALD. Modified Langmuir adsorption isotherm expressions are also used to fit the hydroxyl coverage versus H_2O exposures and Al_2O_3 ALD growth versus H_2O and TMA exposures.

2. Experimental Section

The viscous-flow ALD reactor used in this study has been described in detail previously.[15,16] Briefly, TMA and H_2O are alternately entrained in a N_2 flow by operating gas switching valves. Each reactant enters the reaction zone through a separate 1/4″ stainless steel tube. Figure 1 shows a diagram of the gas switching valves for the H_2O line. During the purge step, most of the 40 sccm of N_2 entering the line flows into the reaction zone. The remaining N_2 is diverted through the regulating valve and purges the small reservoir to a separate pump. During the dose step, the purge valve is closed while the dose valve is opened. H_2O rapidly fills the reservoir before entering the N_2 gas stream through the regulating valve. The dose valve is closed while the purge valve is opened after the set dose time. In this manner, the gas switching valves allow for the rapid turn-on and shut-off of the reactant gases.[16] The TMA gas switching valves are configured in an identical fashion.

The reaction zone consists of a 3.5-cm-diameter flow tube divided into two externally heated zones. The temperatures of each zone were monitored with chromel-alumel thermocouples attached to the outside of the flow tube under the heaters. The temperatures were maintained using PID controllers. The first zone consists of a 15-cm-long preheating zone that was operated at 132 ± 0.5 °C. This zone preheated the N_2 and the reactant gases before they entered the reaction zone. This preheating prevented temperature-induced fluctuations in the QCM signal due to cool reactants entering the flow tube.[26]

The second zone was a 30-cm-long reaction zone that was operated at a temperature of 125 ± 0.5 °C. A Baratron pressure manometer was positioned just behind the reaction zone and monitored the reactor pressure. A total N_2 flow of 200 sccm used in these experiments produced a measured pressure of ∼1 Torr. A QCM inside a custom holder was placed inside the reaction zone. The back side of the crystal was purged with nitrogen to prevent back-side deposition.[16] This back-side purge added ∼0.1 Torr of N_2 pressure to the total nitrogen pressure. An integral thermocouple showed that the QCM temperature during these experiments was 121.9 ± 0.1 °C.

The QCM crystals were AT-cut, 6 MHz quartz crystal with a special low-roughness surface polish. Prior to making any measurements, ∼500 Å of Al_2O_3 ALD was deposited on the QCM crystals to create a reproducible starting surface. A Maxtek TM400 deposition monitor was used to control and monitor the QCM crystal. The resolution of the TM400 mass signal is limited to ∼2 ng/cm^2 due to an apparent rounding error. This rounding error does not affect the TM400 digital output of the period of the QCM crystal.

The period of the QCM crystal was recorded at 100 ms intervals by a personal computer running Labview software. Assuming the acoustic impedance of the deposited film is equal to the acoustic impedance of an AT-cut crystal (i.e., 8.83 × 10^5 g cm^{-2} s^{-1}), the mass deposited per unit area, m, equals[27]

$$m = N_q \cdot \rho_q \cdot \Delta\tau \quad (4)$$

In this equation, $N_q = 1.668 \times 10^5$ Hz-cm is the frequency constant for an AT-cut crystal, $\rho_q = 2.649$ g/cm^3 is the density of the AT-cut crystal,[28] and $\Delta\tau$ is the change in the period. Using eq 4 and the output of the TM400, the mass resolution is ∼0.137 ng/cm^2. The assumption that the acoustic impedance of Al_2O_3

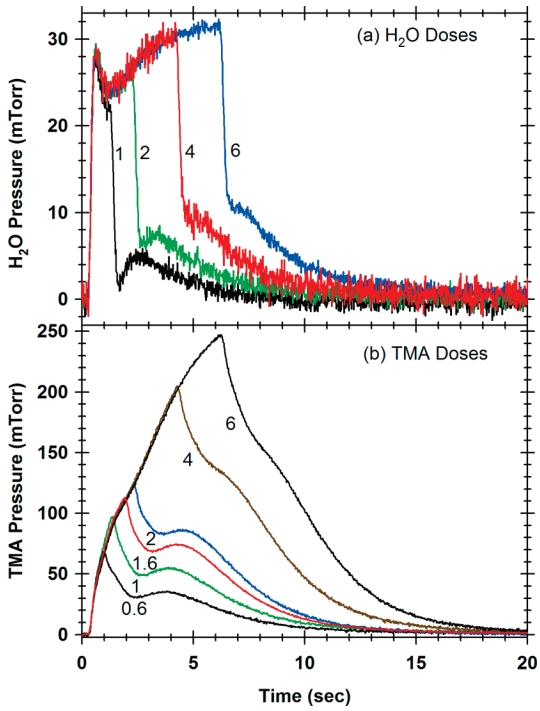

Figure 2. Pressure profiles measured by a capacitance manometer for (a) H_2O and (b) TMA dosing during Al_2O_3 ALD at 125 °C. Pressure profiles are shown for different dosing times in seconds. These pressure profiles were recorded after the surface reactions had reached completion.

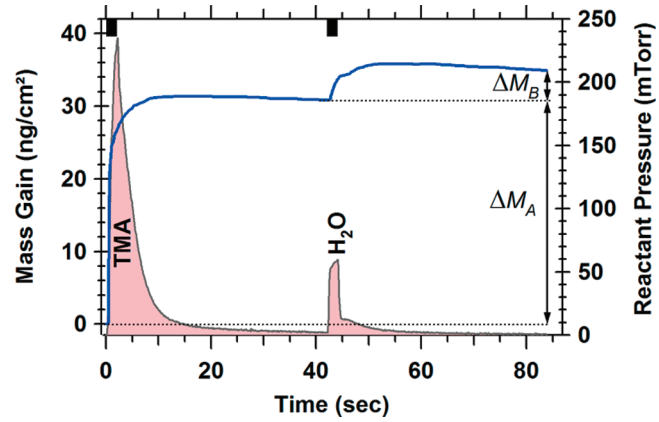

Figure 3. QCM mass gain measured during Al_2O_3 ALD at 125 °C with TMA and H_2O dose times of 2 s indicated by the black bars at the top of the plot. Mass gains during the TMA and H_2O exposures are ΔM_A and ΔM_B, respectively. Solid gray areas show pressure profiles.

ALD equals the acoustic impedance of quartz will lead to an error; however, for a 1% frequency shift, the error in the mass is <2%.[28] The crystal was replaced when the frequency changed by 1% relative to the starting frequency.

Al_2O_3 ALD films were deposited using alternating exposures of H_2O (Fisher, Optima) and TMA (Strem, 98+%). The reactants were maintained at room temperature. These conditions provided vapor pressures of ~20 Torr H_2O and ~11 Torr TMA inside the chemical bottles. The dose times for TMA and H_2O were varied between 0.2 and 6 s with 40 s purges between reactant gases. However, the purge time was increased to 60 s for the 6 s doses. These purge times are significantly longer than purge times used during typical ALD experiments. Monitoring the reactor pressure during the ALD growth revealed that these were the minimum purge times required to return the reactor pressure back to the baseline pressure. During the Al_2O_3 ALD, the QCM period and reactor pressure were recorded at 100 ms intervals.

For each combination of TMA and H_2O dose times, 30 cycles were grown before switching to a different combination of dose times. Changes in the growth rates were observed to occur over the first 5−10 cycles of Al_2O_3 ALD growth for every combination of dose times. These changes are attributed to the coverage of surface sites from the previous 30 cycles of growth. The coverage of surface sites is dependent on the particular dose times. Only data recorded for the last 20 cycles of growth were considered to eliminate this complication.

3. Results and Analysis

A. Pressure Profiles. The total reactant exposure during each reactant dose was quantified using the recorded pressure profiles. The pressure profile during Al_2O_3 ALD consists of three separate components: N_2, $Al(CH_3)_3$ and H_2O reactants and CH_4 reaction products. The relative amounts of $Al(CH_3)_3$ and H_2O reactants consumed and CH_4 reaction products generated are not known. Consequently, the pressure profiles during ALD growth cannot be used to quantify the reactant exposures. Instead, the $Al(CH_3)_3$ and H_2O reactant exposures were quantified by recording the pressures for $Al(CH_3)_3$ and H_2O individually after the surface reaction producing CH_4 reached completion. The pressure profiles were integrated to determine the total exposure in Torr-s after subtracting the N_2 background pressure.

Figure 2 shows the measured pressure profiles in the reactor at 125 °C for the individual $Al(CH_3)_3$ and H_2O reactants. To ensure that these pressure profiles were obtained after the surface reaction reached completion, these pressure profiles were recorded after dosing one of the reactants into the reactor multiple times, separated by a N_2 purge, without dosing the other reactant. Note that the N_2 base pressure was subtracted from each pressure profile. Figure 2a shows the pressure profiles during H_2O doses of 1, 2, 4, and 6 s separated by 40 s N_2 purges. The pressure rises to ~29 mTorr in 300 ms and then begins to fall at ~0.5 s for all the H_2O dose times. For the dose times of 2, 4, and 6 s, the H_2O pressure begins to rise again about 1 s after opening the valve.

For the dose time of 6 s, the H_2O pressure levels off ~5 s after opening the dose valve. For all the dose times, the pressure drops rapidly after the dose valve is closed and the purge valve is reopened. However, after the initial drop, the pressure rises slightly after the purge valve is opened before decaying to the zero level. This additional pressure rise is reduced for longer dose times. The pressure decays following the closing of the dose valves may result from slight changes in the effective pumping speed resulting from the H_2O exposures. In addition, some H_2O may slowly desorb from the surfaces of the reactor and prevent the pressure from reaching the zero level.

Similarly, Figure 2b shows the pressure profiles during TMA doses of 0.6, 1, 1.6, 2, 4, and 6 s separated by 40 s purges. The pressure rise during the TMA dose follows a curve that appears to be identical regardless of dose time. The TMA pressure rises during the entire TMA dose. The TMA pressure drops after the dose valve is closed. During the purge step, the TMA pressure rises slightly for about 2−3 s after the TMA valve is closed for the TMA doses of 0.6, 1, 1.6, and 2 s. For all the TMA doses, the pressure slowly decays to the zero level. This slow decay following the closing of the dose valves again may result from changes in the effective pumping speed resulting from the TMA exposures.

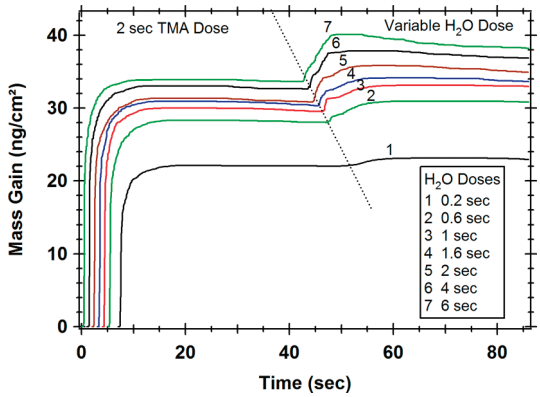

Figure 4. QCM mass gains for Al_2O_3 ALD at 125 °C with a 2 s TMA dose and variable H_2O doses. Each curve is the average of 20 different runs. From left to right the curves are laterally offset in order of decreasing H_2O dose time. The dotted line indicates the start of the H_2O dose.

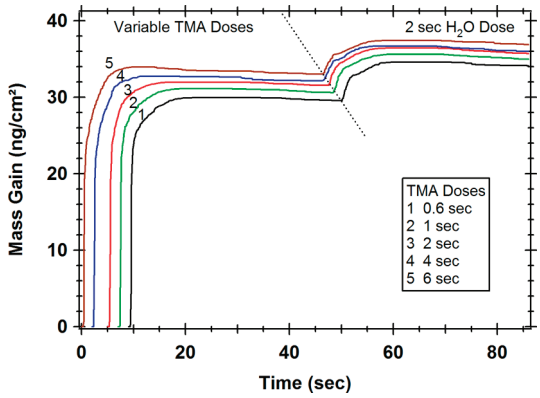

Figure 5. QCM mass gains for Al_2O_3 ALD at 125 °C with a 2 s H_2O dose and variable TMA doses. Each curve is the average of 20 different runs. From left to right, the curves are offset in order of decreasing TMA dose time. The dotted line indicates the start of the H_2O dose.

TMA exists in monomer−dimer equilibrium in the gas phase, and both the monomer and the dimer will be present in the reactor.[29−31] At equilibrium at 120.5 °C, the monomer−dimer equilibrium constant has been measured as $K_d = P_{m\text{-}TMA}^2/P_{d\text{-}TMA} = 1.32 \times 10^{-2}$ mol/L where m-TMA is the monomer and d-TMA is the dimer.[30] This equilibrium constant indicates that a significant fraction of the TMA is present as the dimer. Lower total TMA pressures will increase the relative fraction of monomer. At total TMA pressures of 1, 0.1, and 0.01 Torr at 120.5 °C, the pressure ratios of $P_{m\text{-}TMA}/P_{d\text{-}TMA}$ are approximately 0.11, 0.43, and 1.94, respectively. However, in viscous flow, the mass difference and interconversion between the monomer and dimer should not affect the travel time of TMA through the reactor.

B. Mass Gain versus Time for Variable H_2O and TMA Exposures. Figure 3 shows the mass gain and reactor pressure obtained during a single cycle of Al_2O_3 ALD. The dose times for TMA and H_2O were 2 s, indicated by the solid bars at the top of the graph. The reactant doses were separated by 40 s N_2 purges. The mass gains during the TMA and H_2O doses are indicated by ΔM_A and ΔM_B, respectively. The pressure from the reactants and products obtained after subtracting the N_2 background pressure of ~1 Torr is also shown in Figure 3. Close examination of the pressure profile reveals that the purge time of 40 s is the minimum time required for the pressure to return back to the zero level. Much longer purge times are required for low temperature Al_2O_3 ALD than are typical at higher temperatures.[7]

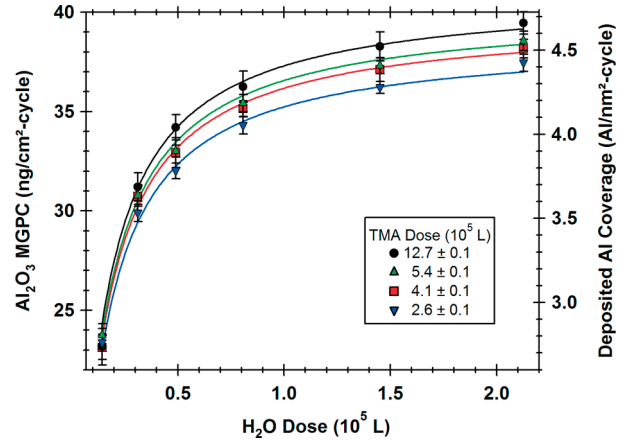

Figure 6. Al_2O_3 MGPC versus H_2O exposure for four different TMA exposures. Solid lines are from a global fit to the data using eq 12.

Typical mass gains obtained for Al_2O_3 ALD with variable H_2O and TMA dose times are shown in Figures 4 and 5, respectively. Each of the curves is the average of 20 ALD cycles. In Figure 4, the H_2O dose time was varied and the TMA dose time was held constant at 2 s. The curves are laterally offset from left to right in order of decreasing H_2O dose. The part of the curves to the left of the dotted line in Figure 4 corresponds to a 2 s TMA dose and a 40 s purge. The start of the H_2O dose is approximately indicated by the dotted line. Most of the H_2O doses are followed by a 40 s purge. However, the H_2O exposure of 6 s is followed by a 60 s purge.

Figure 4 reveals that Al_2O_3 ALD at 125 °C is not completely self-limiting at higher H_2O exposures. The mass gain during the H_2O dose increases for increasing H_2O dose time. In addition, the mass gain increases during the constant TMA doses after the increasing H_2O dose times. Earlier studies have measured Al_2O_3 ALD versus varying H_2O doses at higher temperatures than 125 °C.[32] Slightly larger Al_2O_3 ALD growth rates were observed for larger H_2O doses. This increase was explained in terms of a higher hydroxyl coverage on the Al_2O_3 ALD surface after the larger H_2O doses.[32]

Figure 4 also reveals the importance of sufficiently long purge times. As the H_2O dose times become longer, Figure 4 shows a slight mass loss after the H_2O exposure. This mass loss may result from the desorption of molecularly adsorbed H_2O on the hydroxylated Al_2O_3 surface or from recombinative desorption of hydroxyl species as expressed by the reverse of reaction B2 given by eq 3. The earlier larger growth rates for Al_2O_3 ALD at higher temperatures[32] could have resulted from either higher hydroxyl coverages or molecularly adsorbed H_2O after larger H_2O doses. The purge time after the H_2O dose will play a critical role in defining the time for desorption of molecularly adsorbed H_2O or dehydroxylation of hydroxyl coverage.

The H_2O dose time was constant while the TMA dose time was varied in Figure 5. The curves are again laterally offset from left to right in order of decreasing TMA dose times. The purge time after each reactant was 40 s. The TMA dose begins on the left of the figure; the start of the H_2O dose is indicated by the dotted line. The results show that Al_2O_3 ALD at 125° is not completely self-limiting at higher TMA exposures. For the largest TMA dose of 6 s, the mass gain reaches a maximum at the end of the TMA dose before dropping slightly during the TMA purge step. These results reiterate the importance of sufficiently long purge times. The mass gains were recorded only at the end of purge times to eliminate these transient effects.

The lack of complete self-limiting behavior for both the H_2O and TMA doses suggests that the low temperature of 125 °C

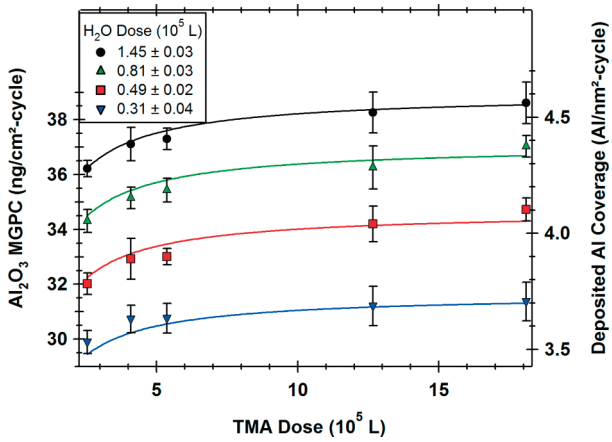

Figure 7. Al_2O_3 MGPC versus TMA exposure for four different H_2O exposures. Solid lines are from a global fit to the data using eq 12.

may be kinetically limiting the reactions. The slower reaction kinetics at lower temperature may require very long exposures for the reactions to reach completion. Consequently, in addition to higher hydroxyl coverages after higher H_2O exposures, another explanation for the lack of self-limiting behavior in Figures 4 and 5 is that extremely long H_2O and TMA exposure times are needed to reach saturation given the kinetic constraints on the surface reactions at 125 °C.

C. Mass Gains per Cycle versus H_2O and TMA Exposure. The MGPC during Al_2O_3 ALD was determined for each cycle by measuring the mass at the end of the H_2O purge and subtracting the mass prior to the TMA dose. Figure 6 displays the MGPC for Al_2O_3 ALD at four different TMA exposures as a function of the H_2O exposure. Similarly, Figure 7 shows the Al_2O_3 MGPC for four different H_2O exposures as a function of the TMA exposure. The H_2O and TMA exposures are plotted in Langmuirs (10^6 $L = 1$ Torr-s). The left-hand axis shows the MGPC. The right-hand axis indicates the number of aluminum atoms deposited per square nanometer per cycle (Al/nm^2-cycle). The deposited aluminum coverage was determined from the well-established stoichiometry of Al_2O_3 ALD.

Figure 6 displays that the Al_2O_3 MGPCs increase quickly with small H_2O doses. The Al_2O_3 MGPCs then increase more slowly versus H_2O dose before nearly reaching a limit at higher H_2O doses. The limiting Al_2O_3 MGPCs are only weakly dependent on the TMA doses. Figure 7 indicates that the Al_2O_3 MGPCs also increase very rapidly with small TMA doses. The Al_2O_3 MGPCs then reach limiting values that are dependent on the H_2O dose. The solid lines in Figures 6 and 7 are fits to the data using a single multivariate fitting function incorporating both the TMA and H_2O exposures. This fitting is described later in Section 4.

Rutherford backscattering has been used previously to determine that Al_2O_3 ALD films grown at 125 °C are stoichiometric Al_2O_3 with no carbon incorporation in the film.[7] However, forward recoil spectrometry revealed a hydrogen concentration of 11% for Al_2O_3 ALD films grown at 125 °C.[7] An FTIR spectroscopy study has also shown earlier that hydroxyl groups remain in the Al_2O_3 ALD film after a saturating TMA exposure.[3] The number of hydroxyl species increases with Al_2O_3 ALD film thickness. In addition, the hydroxyl groups do not undergo isotopic exchange with D_2O and can be eliminated from the film only after annealing above 1000 K.[3] These results indicate that hydroxyls are incorporated in the bulk of the Al_2O_3 ALD film.

Since no carbon is incorporated during Al_2O_3 ALD, the Al_2O_3 MGPCs shown in Figures 6 and 7 can result from only three

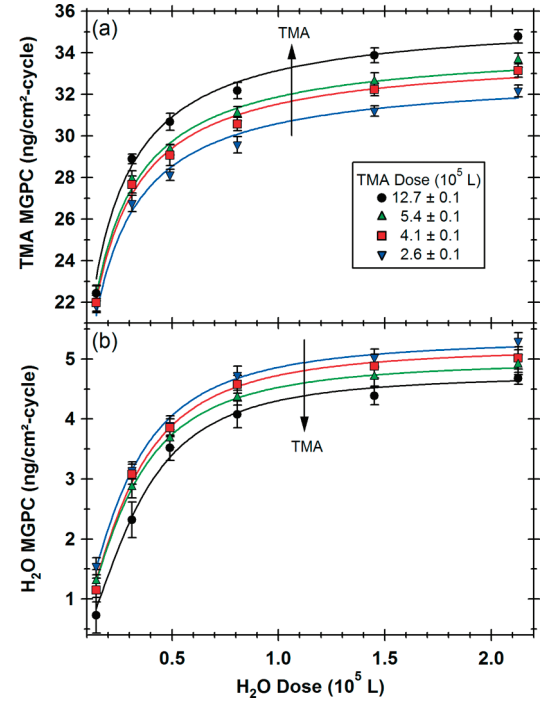

Figure 8. (a) TMA MGPC and (b) H_2O MGPC versus H_2O dose for four different TMA doses. Solid lines are only intended to guide the eye.

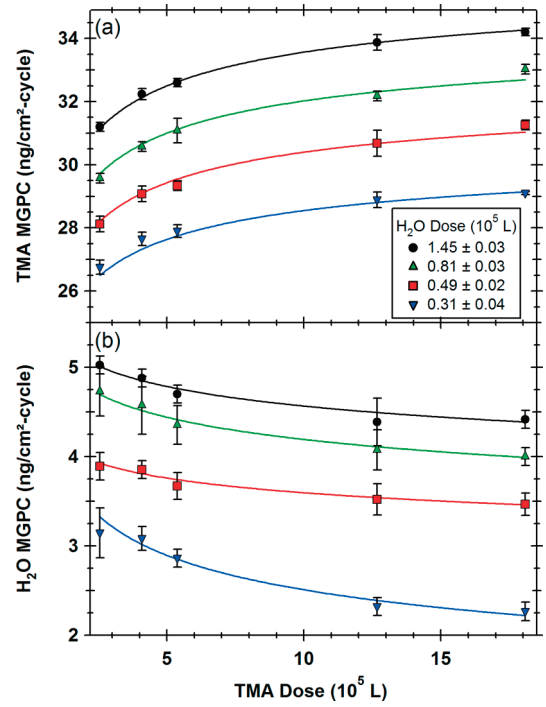

Figure 9. (a) TMA MGPC and (b) H_2O MGPC versus TMA dose for four different H_2O doses. Solid lines are only intended to guide the eye.

atomic species: aluminum, oxygen, and hydrogen. The aluminum coverage deposited per cycle, N_{Al}, can be determined from the measured Al_2O_3 MGPC using

$$N_{Al} = \frac{\Delta M_{Total} \cdot N_A}{\left(m_{Al} + \frac{3}{2}m_O + h \cdot m_H\right)} \quad (5)$$

ΔM_{Total} is the measured MGPC, N_A is Avogadro's number, and m_{Al}, m_O, and m_H are the aluminum, oxygen, and hydrogen molar masses, respectively. h is the fraction of hydrogen included as hydroxyl species in the growing film. The calculated value of N_{Al} is very insensitive to hydrogen incorporation into the film. Assuming the film contained 11% hydrogen decreases the calculated value of N_{Al} by only 0.22%. Because of this insensitivity, all calculations of N_{Al} were made assuming $h = 0$. As shown in Figure 6, N_{Al} ranged from 2.7 to 4.7 Al/nm^2-cycle versus H_2O dose. These N_{Al} values are in good agreement with other experiments that have measured deposited aluminum coverage per cycle of ~4−5 Al/nm^2-cycle at higher temperatures after saturation H_2O doses.[11]

The effects of the H_2O and TMA exposures on the mass gains during each surface reaction were also determined by examining ΔM_A and ΔM_B. Figures 8 and 9 display the MGPCs during the TMA and H_2O doses, respectively, during one Al_2O_3 ALD cycle. The lines in these figures are meant only to guide the eye. Figure 8a and b reveal that the TMA and H_2O MGPCs increase as the H_2O dose increases. Figure 9a shows that the TMA MGPC also increases with increasing TMA exposure. In contrast, Figure 9b shows that the H_2O MGPC decreases with increasing TMA exposure. This complex behavior is caused by the interactions between the TMA and H_2O reactions.

The decrease of H_2O MGPC versus TMA dose in Figure 9b may be caused by more dehydroxylation from the surface at higher hydroxyl coverages. The methyl coverages increase versus TMA dose. These higher methyl coverages would then lead to high initial hydroxyl coverages according to reaction B1 given by eq 2. However, these higher initial hydroxyl coverages may not be stable at 125 °C and may recombine to desorb H_2O via AlOH* + AlOH* → Al−O−Al* + H_2O. This H_2O loss is also expressed by reaction B2 in eq 3 when $x > 1.5$. Because higher TMA doses produce higher methyl coverages that lead to higher hydroxyl coverages, the H_2O MGPC could decrease after higher TMA doses.

D. Hydroxyl and Methyl Coverages versus H_2O and TMA Exposures. The Al_2O_3 ALD surface chemistry is described by reactions A, B1, and B2 in eqs 1−3. However, these reactions can be simplified to just two reaction equations using the known characteristics for Al_2O_3 ALD. First, because the Al/O ratio of the bulk alumina film equals 2:3, 1.5 oxygen atoms must be incorporated per Al surface site. Since water is the only oxygen source in the reactor, 1.5 H_2O molecules must react with each aluminum site. Second, mass spectrometry experiments have shown that CH_4 is the only reaction product.[8] Likewise, Rutherford backscattering experiments have shown there is no carbon incorporation in the Al_2O_3 ALD film.[7] Consequently, all methyl groups remaining on the surface after the TMA dose must react to form CH_4 during the water dose.

Using these characteristics for Al_2O_3 ALD, the mechanism shown in reactions A, B1, and B2 in eqs 1−3 can be simplified to the following two reactions:[12,15]

$$Al(OH)_x^* + Al(CH_3)_3 \rightarrow AlO_xAl(CH_3)_{3-x}^* + xCH_4 \quad (6)$$

$$AlO_xAl(CH_3)_{3-x}^* + 1.5H_2O \rightarrow AlO_{1.5}Al(OH)_x^* + (3-x)CH_4 \quad (7)$$

In these reactions, hydrogen atoms from H_2O remove the methyl groups from $Al(CH_3)_{3-x}^*$ as CH_4. The remaining hydrogen atoms from H_2O produce $Al(OH)_x^*$ species. Equations 6 and 7 cannot describe hydrogen incorporation in the Al_2O_3 ALD film. However, neglecting the hydrogen incorporation is only a minor error for the mass changes during Al_2O_3 ALD.

The MGPC for the TMA reaction, ΔM_A, described by eq 6 is

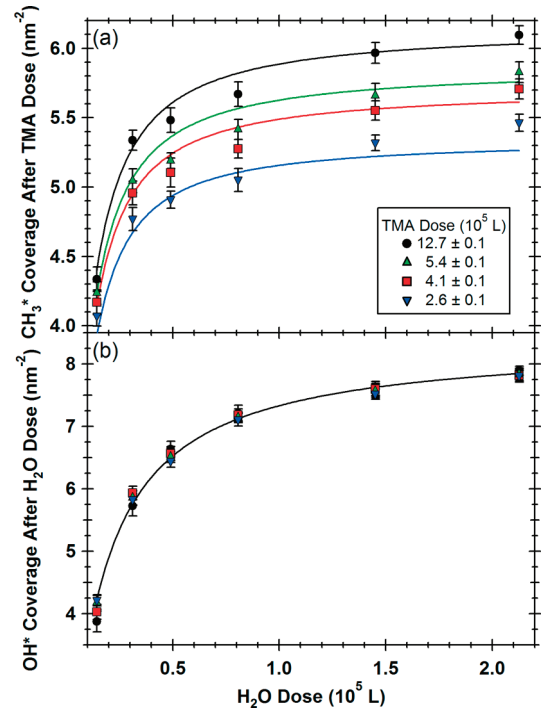

Figure 10. (a) CH_3^* coverage after TMA dose and (b) OH* coverage after H_2O dose versus H_2O dose for four different TMA doses. The lines fit to the CH_3^* coverages in panel a are from eq 10. The line fit to the OH* coverage in panel b is from eq 11.

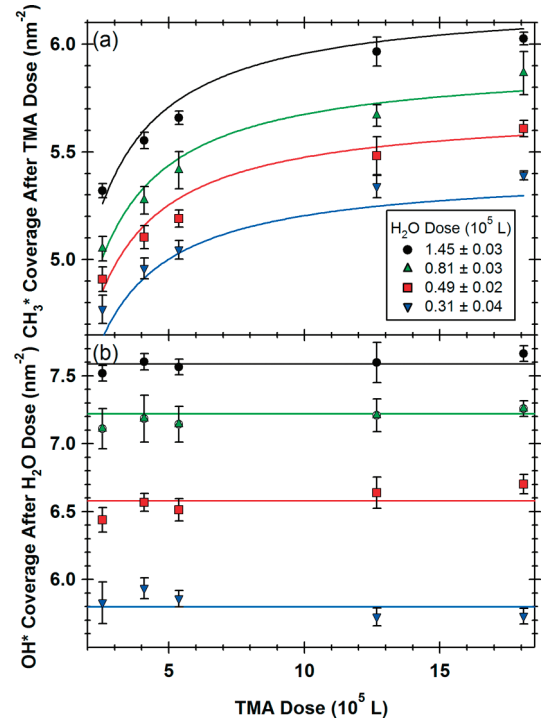

Figure 11. (a) CH_3^* coverage after TMA dose and (b) OH* coverage after H_2O dose versus TMA dose for four different H_2O doses. The lines fit to the CH_3^* coverages in panel a are from eq 10. The line fit to the OH* coverage in panel b is from eq 11.

$$\Delta M_A = N_{Al}(m_{TMA} - x \cdot m_{CH_4}) \quad (8)$$

where N_{Al} is the deposited aluminum coverage per cycle and m_{TMA} and m_{CH_4} are the molar masses of TMA and CH_4, respectively. x is the number of hydroxyls that react per Al atom deposited on the surface. By combining eqs 5 and 8 with $h = 0$, the coverage of hydroxyl species, N_{OH}, after the H_2O reaction is given by

$$N_{OH} = N_{Al} \cdot x = \frac{N_{Al} \cdot m_{TMA}}{m_{CH_4}} - \frac{\Delta M_A}{m_{CH_4}} \quad (9)$$

Similarly, the coverage of methyl species, N_{CH_3}, after the TMA reaction described by eq 6 is given by

$$N_{CH_3} = 3N_{Al} - N_{OH} \quad (10)$$

Figure 10 displays the CH_3^* and OH* coverages after the TMA and H_2O reactions, respectively, as a function of the H_2O exposure for various TMA doses. Figure 11 shows the CH_3^* and OH* coverages after the TMA and H_2O reactions, respectively, as a function of the TMA exposure for various H_2O doses. The CH_3^* coverage after the TMA dose shown in Figures 10a and 11a is clearly dependent on both the TMA and H_2O exposures. The lines are fits to the methyl coverage. The OH* coverages after the H_2O dose for the four different TMA exposures shown in Figure 10b are all nearly identical. The OH* coverage after the H_2O dose increases with increasing H_2O exposure. Figure 11b shows that the OH* coverage after the H_2O dose is constant with respect to the TMA dose. The straight lines indicate the average hydroxyl coverage for each of the four different H_2O exposures.

4. Fitting Using Modified Langmuir Adsorption Isotherm Expressions

A. Hydroxyl Coverage. The dependence of the Al_2O_3 ALD growth rate on the hydroxyl coverage at temperatures higher than 125 °C was discussed in a recent review paper.[11] At growth temperatures of 150−250 °C, the deposited aluminum per cycle was found to depend linearly on the surface hydroxyl coverage. Similarly, the methyl coverage after the TMA reaction was also found to depend linearly on the hydroxyl coverage. Because of the importance of the hydroxyl coverage, analysis of Al_2O_3 ALD at 125 °C will first discuss the dependence of the hydroxyl coverage on the reactant exposures. The hydroxyl coverage on the surface was determined assuming that eqs 6 and 7 accurately describe the Al_2O_3 ALD process.

Figure 10b indicates that the hydroxyl coverage on the surface after the H_2O dose depends only on the H_2O exposure. Figure 11b shows that the hydroxyl coverage is constant with respect to the TMA dose. However, Figure 7 reveals that the deposited aluminum coverage per cycle does depend slightly on the TMA dose. Therefore, the hydroxyl coverage after the H_2O dose apparently does not depend on the deposited aluminum coverage per cycle. Figure 11a and b reveals that the OH* coverage does not depend on the CH_3^* coverage. Since the hydroxyl coverage after the H_2O dose is independent of the surface produced by the TMA dose, the hydroxyl coverage can be calculated using only the H_2O exposure.

The data in Figure 10b for the OH* coverage after the H_2O dose were fit using a modified Langmuir adsorption isotherm

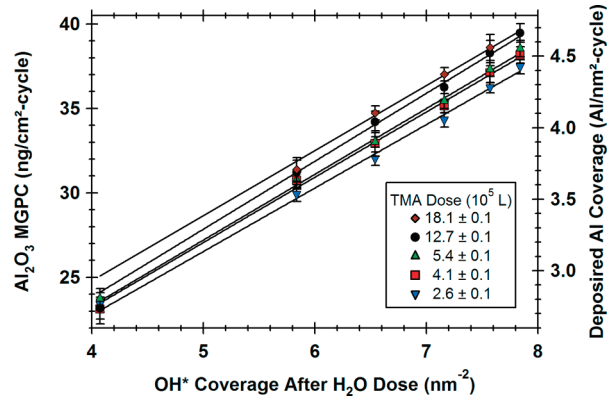

Figure 12. Al_2O_3 MGPC versus OH* coverage after H_2O dose for five different TMA doses. OH* coverages are calculated from eq 9. The solid lines are linear fits using a single y-intercept and different slopes.

expression. The Langmuir adsorption isotherm is applied to the equilibrium of surface coverage and adsorbate pressure assuming that each adsorbate occupies a single surface site.[33] In these ALD experiments, the adsorbate reacts with the surface, the pressure was not constant, and there is no equilibrium. However, the form of the Langmuir adsorption isotherm expression can still be used to fit the hydroxyl coverage versus H_2O exposure. Exposure replaces pressure in this modified Langmuir adsorption isotherm expression:[33]

$$S = \frac{S_0}{\left(1 + \frac{L^*}{L_{H_2O}}\right)} \quad (11)$$

In this equation, S is the measured hydroxyl coverage, L_{H_2O} is the H_2O exposure in Langmuirs, and S_0 is the hydroxyl surface coverage corresponding to the saturation coverage.

In the standard Langmuir adsorption isotherm equation, $L^* = 1/K_{eq}$ where K_{eq} is the equilibrium constant $K_{eq} = k_a/k_d$ where k_a and k_d are the adsorption and desorption rate constants. In the modified Langmuir adsorption isotherm expression, L^* can be viewed as the H_2O exposure that yields $S = S_0/2$; that is, one-half of the complete hydroxyl coverage, S_0. The hydroxyl coverage grows progressively with H_2O exposures before reaching a saturation coverage after long H_2O exposures. The fit using eq 11 is shown by the solid line in Figure 10b.

This excellent fit suggests that H_2O reactive adsorption occurs with a probability that is dependent on the availability of unreacted $AlCH_3^*$ surface sites. For Langmuir adsorption, the adsorption probability is expressed as $(1 - \Theta)$, where Θ is the coverage of reacted AlOH* surface sites. Θ is a normalized coverage, and complete coverage is $\Theta = 1$. The H_2O reactive adsorption versus H_2O exposure mirrors the adsorption/desorption equilibrium during Langmuir adsorption versus adsorbate pressure.

From the fit, the maximum absolute hydroxyl surface coverage at 125 °C is $S_0 = 8.37 \pm 0.09$ nm^{-2}, and the H_2O exposure required to achieve 50% hydroxyl coverage half-exposure is $L^* = 1.41 \pm 0.04 \times 10^4$ L. In comparison, the full monolayer hydroxyl coverage on alumina powders at 100 °C is ~12.5 nm^{-2}.[34−36] The hydroxyl coverage on alumina powders after annealing at 200 °C is ~9 nm^{-2}.[34] The maximum hydroxyl coverage of $S_0 = 8.37 \pm 0.09$ nm^{-2} at 125 °C is in reasonable agreement with the previously measured hydroxyl coverages on alumina powders. The slightly larger hydroxyl coverages

on the alumina powders may be attributed to the differences between the planar and powder samples.

B. Al_2O_3 Mass Gain Per Cycle. Previous investigations at temperatures higher than 125 °C have shown that the number of aluminum atoms deposited during the TMA dose increases linearly with the hydroxyl coverage.[11,37] For Al_2O_3 ALD at 125 °C, a plot of the Al_2O_3 MGPC versus the hydroxyl coverage after the H_2O dose is shown in Figure 12. The deposited Al coverage per cycle is shown on the right axis. The symbols are the measured data using five different TMA doses. The Al_2O_3 MGPC increases very linearly with the OH* coverage. The solid lines are linear fits to data using a constant *y*-intercept and variable slopes.

The *y*-intercept defines the deposited aluminum coverage per cycle on a completely dehydroxylated Al_2O_3 surface. From the fits in Figure 12, the deposited aluminum coverage per cycle for the dehydroxylated surface equals 0.91 ± 0.07 nm^{-2}. The slope increases slightly with increasing TMA exposure. The slope (Al_2O_3 MGPC)/(OH* coverage) increases from 0.44 ± 0.01 at a TMA dose of 2.6×10^5 L to 0.48 ± 0.01 at a TMA dose of 12.7×10^5 L.

Previous measurements of complete TMA adsorption have been performed on powdered alumina and silica with different initial hydroxyl densities.[11,37] The deposited Al coverage per cycle versus OH* coverage was linear with a *y*-intercept of 1.68 ± 0.09 nm^{-2} and a slope of 0.37 ± 0.02.[11,37] These previous reports for the slope are in good agreement with our measured slopes of 0.44−0.48. The different *y*-intercepts may reflect the difference between the planar substrates used in the current experiments and the porous substrates utilized in the earlier measurements.

The Al_2O_3 MGPC is a linear function of the hydroxyl coverage. The hydroxyl coverage depends on the H_2O exposure according to the modified Langmuir adsorption isotherm expression given in eq 11. A similar form for ΔM_{Total} can be constructed on the basis of contributions from H_2O and TMA exposures. A trial function for ΔM_{Total} versus H_2O and TMA exposures is

$$\Delta M_{Total} = \frac{M_{max}}{\left(1 + \frac{L^*_{H_2O}}{L_{H_2O}}\right)\cdot\left(1 + \frac{L^*_{TMA}}{L_{TMA}}\right)} \qquad (12)$$

where L_{H_2O} and L_{TMA} are the H_2O and TMA exposures in Langmuirs, respectively. M_{Max} is the maximum mass gain. Similar to L^* in eq 11, $L^*_{H_2O}$ and L^*_{TMA} can be viewed as the H_2O and TMA "half exposures". When the H_2O and TMA exposures are equal to their respective "half-exposures", the total mass gain corresponds to 25% of the maximum mass gain.

All the data shown in Figures 6 and 7 were fit using eq 12 to determine the values of the M_{Max}, $L^*_{H_2O}$ and L^*_{TMA}. The fit using eq 12 to the data in Figures 6 and 7 is quite good. The average difference between the measured and calculated values is ~1%. From this fit, $M_{Max} = 41.6 \pm 0.3$ ng/cm^2-cycle. The maximum mass gain corresponds to a deposited Al coverage per cycle of 4.91 ± 0.03 nm^{-2} cycle^{-1}. Previous experiments measured a maximum Al_2O_3 growth rate at 125 °C equal to 39 ng/cm^2-cycle.[7] This previous measurement is in good agreement with $M_{Max} = 41.6 \pm 0.3$ ng/cm^2-cycle. The half-exposures for H_2O and TMA are $L^*_{H_2O} = 9.8 \pm 0.3 \times 10^3$ L and $L^*_{TMA} = 1.9 \pm 0.2 \times 10^4$ L, respectively.

This fit of the modified Langmuir adsorption isotherm expression to the data in Figures 6 and 7 suggests that H_2O and TMA reactive adsorption occurs with probabilities that are dependent on the availability of unreacted $AlCH_3^*$ and AlOH* sites, respectively. The fits again argue that the reactive adsorption probabilities are proportional to $(1 - \Theta)$, where Θ is the coverage of either reacted $AlCH_3^*$ sites during H_2O adsorption or reacted AlOH* sites during TMA adsorption.

5. Conclusions

QCM measurements were used to examine Al_2O_3 ALD growth using TMA and H_2O at 125 °C. The Al_2O_3 ALD MGPCs were measured versus TMA and H_2O exposures. The MGPCs for the individual TMA and H_2O reactions were also measured versus TMA and H_2O exposures. The Al_2O_3 MGPC increased with increasing H_2O exposures at a fixed TMA exposure. The Al_2O_3 MGPC also increased with increasing TMA exposure at a fixed H_2O exposure. The QCM studies revealed that neither the TMA nor the H_2O reactions were completely self-limiting. This behavior may be attributed to the slower reaction kinetics for the TMA and H_2O surface at lower temperature.

The Al_2O_3 MGPCs increased rapidly after small H_2O doses and slowly reached a limiting value that was not very dependent on the TMA dose. The Al_2O_3 MGPCs also increased rapidly after small TMA doses and different limiting values were obtained for different H_2O doses. The TMA MGPCs increased for higher TMA exposures for all H_2O exposures. On the other hand, the H_2O MGPC decreased for higher TMA exposures at all H_2O exposures. More dehydroxylation at higher hydroxyl coverages may explain this decrease. The higher hydroxyl coverages after H_2O exposures result from higher methyl coverages after higher TMA exposures. The hydroxyl coverage after the H_2O exposure was dependent only on the H_2O exposure. The Al_2O_3 MGPC was linearly dependent on the hydroxyl coverage after the H_2O dose.

The hydroxyl coverage versus the H_2O exposures and the Al_2O_3 MGPC versus the H_2O and TMA exposures were fit using modified Langmuir adsorption isotherm expressions. These fits suggest that reactant adsorption during the H_2O and TMA exposures occurs with a probability that is dependent on $(1 - \Theta)$, where Θ is the coverage of reacted surface sites. These results should be useful for understanding and modeling low temperature Al_2O_3 ALD. Many applications result from low temperature Al_2O_3 ALD on organic, polymeric, and biological substrates.

Acknowledgment. This work was funded by the Air Force Office of Scientific Research. Additional funding was provided by Sandia National Laboratories in Albuquerque.

References and Notes

(1) George, S. M.; Ott, A. W.; Klaus, J. W. *J. Phys. Chem.* **1996**, *100*, 13121.
(2) Suntola, T. *Thin Solid Films* **1992**, *216*, 84.
(3) Dillon, A. C.; Ott, A. W.; Way, J. D.; George, S. M. *Surf. Sci.* **1995**, *322*, 230.
(4) Ferguson, J. D.; Weimer, A. W.; George, S. M. *Thin Solid Films* **2000**, *371*, 95.
(5) Ferguson, J. D.; Weimer, A. W.; George, S. M. *Chem. Mater.* **2004**, *16*, 5602.
(6) Groner, M. D.; Elam, J. W.; Fabreguette, F. H.; George, S. M. *Thin Solid Films* **2002**, *413*, 186.
(7) Groner, M. D.; Fabreguette, F. H.; Elam, J. W.; George, S. M. *Chem. Mater.* **2004**, *16*, 639.

(8) Juppo, M.; Rahtu, A.; Ritala, M.; Leskelä, M. *Langmuir* **2000**, *16*, 4034.
(9) Ott, A. W.; Klaus, J. W.; Johnson, J. M.; George, S. M. *Thin Solid Films* **1997**, *292*, 135.
(10) Ott, A. W.; McCarley, K. C.; Klaus, J. W.; Way, J. D.; George, S. M. *Appl. Surf. Sci.* **1996**, *107*, 128.
(11) Puurunen, R. L. *J. Appl. Phys.* **2005**, *97*.
(12) Rahtu, A.; Alaranta, T.; Ritala, M. *Langmuir* **2001**, *17*, 6506.
(13) Higashi, G. S.; Fleming, C. G.*Appl. Phys. Lett.* **1989**, *55*, 1963.
(14) Soto, C.; Tysoe, W. T. *J. Vac. Sci. Technol., A* **1991**, *9*, 2686.
(15) Wind, R. A.; Fabreguette, F. H.; Sechrist, Z. A.; George, S. M. *J. Appl. Phys.* **2009**, *105*, 074309.
(16) Elam, J. W.; Groner, M. D.; George, S. M. *Rev. Sci. Instrum.* **2002**, *73*, 2981.
(17) Mayer, T. M.; Elam, J. W.; George, S. M.; Kotula, P. G.; Goeke, R. S. *Appl. Phys. Lett.* **2003**, *82*, 2883.
(18) Ritala, M.; Leskela, M.; Dekker, J. P.; Mutsaers, C.; Soininen, P. J.; Skarp, J. *Chem. Vap. Deposition* **1999**, *5*, 7.
(19) Wilson, C. A.; Grubbs, R. K.; George, S. M. *Chem. Mater.* **2005**, *17*, 5625.
(20) *HSC Chemistry 5.1*; Outokumpu Research Oy: Pori, Finland.
(21) Knez, M.; Kadri, A.; Wege, C.; Gosele, U.; Jeske, H.; Nielsch, K. *Nano Lett.* **2006**, *6*, 1172.
(22) Lee, S. M.; Pippel, E.; Gosele, U.; Dresbach, C.; Qin, Y.; Chandran, C. V.; Brauniger, T.; Hause, G.; Knez, M. *Science* **2009**, *324*, 488.
(23) Carcia, P. F.; McLean, R. S.; Reilly, M. H.; Groner, M. D.; George, S. M. *Appl. Phys. Lett.* **2006**, *89*, 031915.
(24) Dameron, A. A.; Davidson, S. D.; Burton, B. B.; Carcia, P. F.; McLean, R. S.; George, S. M. *J. Phys. Chem. C* **2008**, *112*, 4573.
(25) Groner, M. D.; George, S. M.; McLean, R. S.; Carcia, P. F. *Appl. Phys. Lett.* **2006**, *88*, 051907.
(26) Rocklein, M. N.; George, S. M. *Anal. Chem.* **2003**, *75*, 4975.
(27) Theory of Operation. In *Maxtek TM-350/400 Operation and Service Manual for Model TM-350/400 Maxtek Thickness Monitor*, 10th ed.; Maxtek, Inc.: Santa Fe Springs, California, 2004.
(28) Benes, E. *J. Appl. Phys.* **1984**, *56*, 608.
(29) Hay, J. N.; Hooper, P. G.; Robb, J. C. *J. Organomet. Chem.* **1971**, *28*, 193.
(30) Henricks, Ch.; Eyman, D. P. *Inorg. Chem.* **1967**, *6*, 1461.
(31) Laubengayer, L. W.; Gilliam, W. F. *J. Am. Chem. Soc.* **1941**, *63*, 477.
(32) Matero, R.; Rahtu, A.; Ritala, M.; Leskela, M.; Sajavaara, T. *Thin Solid Films* **2000**, *368*, 1.
(33) Masel, R. I. *Principles of Adsorption and Reaction on Solid Surfaces*, 1st ed.; John Wiley & Sons, Inc.: New York, 1996.
(34) Knozinger, H.; Ratnasamy, P. *Catal. Rev. Sci. Eng.* **1978**, *17,* 31.
(35) Peri, J. B. *J. Phys. Chem.* **1965**, *69*, 211.
(36) Peri, J. B. *J. Phys. Chem.* **1965**, *69*, 220.
(37) Puurunen, R. L. *Appl. Surf. Sci.* **2005**, *245*, 6.

JP9049268